Appl Phys B (2009) 94: 715–723
DOI 10.1007/s00340-009-3363-9

Applied Physics B
Lasers and Optics

High-resolution infrared polarization spectroscopy and degenerate four wave mixing spectroscopy of methane

K. Richard · P. Ewart

Received: 16 June 2008 / Revised version: 26 November 2008 / Published online: 24 January 2009

Abstract High-resolution infrared polarization spectroscopy (IR-PS) and degenerate four wave mixing (IR-DFWM) spectroscopy of methane using a diode-seeded modeless laser (DSML) system are reported. Mid-infrared radiation around 3.3 μm is generated by difference frequency mixing of the single-mode output of the DSML around 0.634 μm with the frequency-doubled output of a single-mode Nd:YAG pump laser at 0.532 μm. Polarization spectroscopy signals in the forward geometry were generated in methane at around 5 Torr pressure. IR-PS spectra were recorded with a typical signal-to-noise ratio of 150:1 with methane pressures of at least 1 Torr. The line shape of the IR-PS signals was analysed to measure pressure broadening induced by nitrogen buffer gas yielding a value of 6.3 ± 1.5 MHz Torr^{-1}. IR-DFWM spectra of methane were generated in the counter-propagating pump geometry yielding Doppler-free signals with signal-to-noise ratios of typically 650:1. Signals were obtained at methane pressures down to less than 10 mTorr. A comparison of IR-PS and IR-DFWM is made indicating that IR-DFWM has some advantages over IR-PS in this spectral region in terms of sensitivity, signal-to-noise ratio and ease of use. The results illustrate the utility of the DSML for high-resolution nonlinear spectroscopy in the mid infrared.

PACS 42.62.Fi · 42.72.Ai

K. Richard · P. Ewart (✉)
Clarendon Laboratory, University of Oxford, Parks Road,
Oxford OX1 3PU, UK
e-mail: p.ewart@physics.ox.ac.uk
Fax: +44-1865-272375

1 Introduction

Nonlinear spectroscopic techniques offer significant advantages in a variety of applications including combustion and plasma diagnostics, chemical and process analysis, gas sensing and flow measurement. These advantages include providing a signal in the form of a coherent, laser-like beam which facilitates discrimination against background noise from luminous environments such as flames or hot plasmas [1, 2]. These advantages are especially valuable in the infrared spectral region where thermal background can be intense. Mid-infrared detectors are also generally less sensitive than those for visible radiation and so the ability to focus the signal to a small area yields a further advantage. The mid-infrared region is spectroscopically rich since it is here that many important molecules and radicals have their 'fingerprint' spectra. In particular, the fundamental CH stretch mode around 3 μm characterises the energy level structure of many hydrocarbon species. Ro-vibrational transitions in this spectral region exhibit very low spontaneous emission probability and so detection by fluorescence methods is usually prohibited. Absorption methods lack spatial resolution. There is therefore a premium on developing detection techniques that provide spatial and temporal resolution together with species and state selectivity with sensitivity to trace concentrations. Methods based on coherent or stimulated processes and nonlinear techniques such as polarization spectroscopy, PS, and degenerate four wave mixing, DFWM, are the most promising nonlinear candidates for detection of minor species in this spectral region [3, 4]. Infrared polarization spectroscopy, IR-PS, has been demonstrated for the detection of CO_2 [5], OH [6], H_2O [7], CH_4 [8] and C_2H_2 [9] and infrared DFWM, IR-DFWM, has also been applied to spectroscopy of the polyatomic molecules CH_4 and C_2H_2 [3, 10].

Progress in nonlinear laser spectroscopy in the infrared has been hampered by the lack of suitable and readily available laser sources. Nonlinear optical techniques demand high peak powers that are not usually available from c.w. lasers and so pulsed lasers are needed. On the other hand, spectroscopy in the mid infrared often demands high spectral resolution since the spectra are often congested. If species- and state-specific excitation is to be achieved then a narrow spectral bandwidth is demanded of the laser and ideally the source should provide a single longitudinal mode. Such narrow bandwidths are however not usually provided by high-power pulsed lasers.

A practical problem for quantitative laser spectroscopy in the infrared arises from the mode structure of most laboratory lasers. The spectrum of a conventional laser consists of a group of longitudinal modes spaced in frequency by the free spectral range, $c/2L$, where c is the speed of light and L is the laser cavity length. For typical laboratory pulsed dye lasers the mode spacing will be ~500 MHz. Although the envelope of the laser spectrum is tuned by some frequency-selective element in the cavity, the frequency of the individual modes remains fixed. Spectral line widths of molecular absorption features in the mid infrared can be of the order of 10–100 MHz. It is possible then that a molecular resonance frequency may fall between the frequencies of adjacent modes and so it will not be excited even though the envelope of the laser spectrum is tuned across the resonance frequency. Even when the molecular transition spans one or several longitudinal modes the excitation will be determined by the positions of modes relative to the transition line centre. The resulting signal will then be subject to large fluctuations arising from random fluctuations of the laser mode intensities and frequencies. This effect places an even greater premium on having a single longitudinal mode that can be continuously tuned in frequency across a significant range of the spectrum.

Mid-infrared radiation may be generated by difference frequency generation (DFG) using pulsed dye lasers and Nd:YAG pump lasers. The line widths of such systems are usually limited to around 0.1 cm^{-1} or 3 GHz and are subject to the problems arising from fixed mode frequencies detailed above. Mid-infrared radiation is readily generated by optical parametric processes. Tuneable single-mode operation of optical parametric oscillators, OPOs, is achieved by seeding with a single-mode laser such as a colour centre, Ti:sapphire or diode laser and high power may be obtained by use of optical parametric amplifiers, OPAs [11–13]. Orr and co-workers have developed injection-seeded OPOs and OPAs for applications in high-resolution spectroscopy [14–17]. Alternative seeding strategies for OPO and OPG (Optical Parametric Generation) systems have been developed and Lucht and co-workers have used such systems with OPAs to produce high power for nonlinear spectroscopy [18–20].

Raman shifting of the output of a pulsed alexandrite laser when seeded by a single-mode diode laser provides a promising alternative [21]. This system is however complex, quite expensive, has limited single-mode tunability and reaches a limited range of the infrared region.

The diode-seeded modeless laser, DSML, has been developed to provide high-power, continuously tunable, single-mode radiation for applications such as linear and nonlinear spectroscopy [22]. It has been successfully applied to high-resolution cavity ring-down spectroscopy [23] and degenerate four wave mixing [24] of flame OH in the ultraviolet by frequency doubling the visible-wavelength output. The system has been recently improved and applied to polarization spectroscopy of molecular iodine in the visible spectral region [25]. The improved system uses an internal, passive, frequency-locking technique resulting in an effective wide single-mode tuning range without mode hops. In the present work this improved version of the DSML is applied for the first time for nonlinear spectroscopy in the mid infrared. Radiation around 3.3 μm was generated by DFG using the DSML output at 0.634 μm and residual energy from the frequency-doubled Nd:YAG laser at 0.532 μm used to pump the DSML.

Infrared polarization spectroscopy (IR-PS) has been reported using a conventional Nd:YAG-pumped dye laser system and DFG in which wide spectral scans of IR-PS in methane were achieved [8]. The line width of this system is limited by the bandwidth of the pulsed dye laser of ~0.04 cm^{-1} and relative intensities would be affected by mode effects in the dye laser oscillator. In the present work, the DSML, having a line width of 0.006 cm^{-1}, is used to generate the mid-IR radiation by DFG. The system was then used to generate IR-PS of methane with a significant increase in resolution. Polarization spectroscopy provides a stringent test of the laser system in terms of the amplitude and frequency stability of the output and the pointing and polarization stability of the beam. Small changes in beam direction or polarization orientation can lead to distortion of the line shape arising from effective uncrossing of the polarizers used in producing the signal.

High-resolution infrared DFWM was first demonstrated using a commercial single-mode OPO that is no longer available [3]. The present work applies a DSML to generate mid-infrared radiation by DFG. It is possible to construct a DSML using commercially available products and so this opens the possibility of reliably generating high-power, single-mode radiation in the mid infrared. In the present work a DSML is used with DFG to generate IR-DFWM signals in methane for comparison with the IR-PS technique.

In what follows the apparatus, laser system and experimental methods are briefly described. High-resolution studies using IR-PS of methane are then reported and also the results of detecting methane using IR-DFWM with the same

laser system. The relative merits of the two techniques are then discussed in terms of sensitivity, signal-to-noise achievable, ease of use and data analysis.

2 Apparatus and experimental procedure

The experimental arrangements for IR-PS and IR-DFWM are shown in Fig. 1, which also shows the essential similarity of the optical layouts involved. The conventional arrangement for polarization spectroscopy was used as described in the literature and shown schematically in Fig. 1a [26, 27]. Although the 'counter-propagating' geometry, with pump and probe beams crossing the sample in opposite directions, offers an effectively 'Doppler-free' spectroscopy, the experimentally simpler, forward arrangement was chosen in this test of the DSML system. The counter-propagating geometry is actually 'Doppler selective' in that it selects the subgroup of molecules having essentially zero velocity parallel to the incident laser beams. Consequently, the signals are inherently weaker than those obtained in the forward geometry where the entire velocity distribution is probed. Doppler broadening is also usually not the dominant broadening mechanism in the mid-infrared region. The 'counter-propagating' geometry was however adopted for the IR-DFWM experiments as shown in Fig. 1b since the reduction in signal by the Doppler selection was found not to be a problem. This arrangement was found to be both experimentally simpler and provided improved resolution by reducing the Doppler-broadening component of the line shape.

Methane was contained in a 10-cm-long, stainless steel, cell fitted with angled windows to avoid etalon effects caused by surface reflections. The pressure in the cell was measured using a capacitance manometer (MKS Baratron) and buffer gas (nitrogen) could be introduced to vary the degree of pressure broadening. The construction of the DSML has been described elsewhere and is outlined only briefly here for convenience [22, 25]. The beam from a c.w. external cavity diode laser (New Focus 6202) operating between 632 and 639 nm is used to seed a modeless laser [28] acting as a narrow-bandwidth amplifier. Radiation from a frequency-doubled, seeded single-mode, Nd:YAG laser (Coherent 8010) was split to provide pump energy for the DSML and for the DFG process. A total of approximately 180 mJ of energy was used to pump the modeless laser and two further amplifier stages. The resulting output of the DSML after the two stages of longitudinally pumped amplifiers consisted of a pulse with energy up to 40 mJ, duration 5 ns and bandwidth 0.006 cm^{-1}. The bandwidth was measured previously using a Fabry–Perot interferometer having an instrumental width of 39 MHz or 0.0013 cm^{-1} (Technical Optics).

The DSML was improved over the system reported previously [22] by the addition of a novel frequency-locking

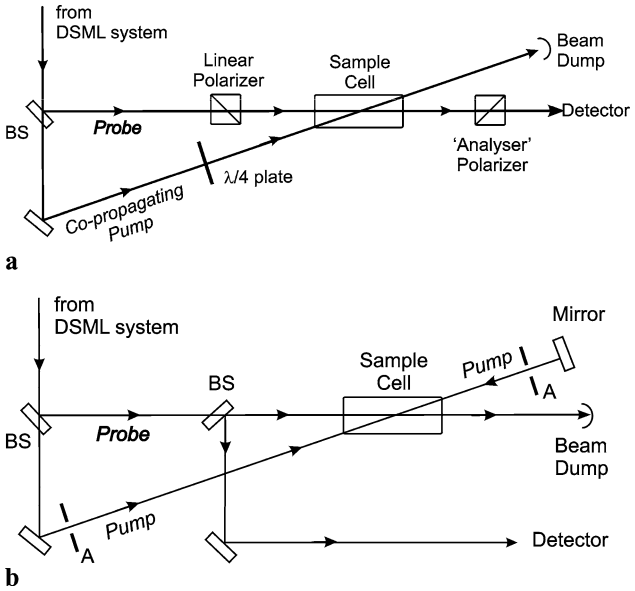

Fig. 1 **a** Schematic of experimental layout for IR-PS using the 'forward' geometry. The probe beam is created by splitting a small fraction of the incoming laser pulse at a beam splitter, BS. The pump beam co-propagates with the probe at a small angle crossing the probe beam in the sample cell containing methane and buffer gas. The probe passes through two crossed Glan–Thomson polarizers so that the detector registers a signal depending on the polarization rotation induced by the circularly polarized pump beam. **b** The layout for IR-DFWM showing the similarity to that for IR-PS. The two counter-propagating pump beams are created and overlapped easily by retro-reflecting the forward pump beam through a system of two apertures, A. The signal beam generated by phase-conjugate reflection in the interaction region is picked off by a beam splitter, BS

system [25]. This system controlled the tuning of the DSML such that it followed the frequency tuning of the diode laser and compensated automatically for any mode hopping. The result of this improved frequency-scanning system is that the output energy is maximized, the line width minimized and beam-pointing stability of the DSML is maintained as the laser is tuned. Using this system it is possible to tune the laser over a wide spectral range (~60 cm^{-1}) whilst maintaining single-mode operation. The tuning range is ultimately limited only by the gain bandwidth of the seeding diode laser or the amplifier dye. Furthermore, it is possible by appropriate programming of the tuning elements to scan rapidly over some spectral regions and to then scan slowly, with high resolution, over selected regions containing spectral lines of interest.

The spectrum and absolute frequency of the DSML output were monitored using a multiple Fizeau interferometer (Cluster LM007) having a precision of ±0.003 cm^{-1}. Once the Nd:YAG laser was thermally stabilized the wavenumber of the frequency-doubled Nd:YAG output was found to be stable within the line width of ~0.006 cm^{-1} during the time taken to acquire data but the absolute value could vary owing to longer term drift of the cavity. Additional drifts in the

absolute calibration of the Fizeau interferometer resulted in a degree of uncertainty in the absolute value of the mid-IR radiation generated by DFG. The wavelength measurement of the DSML output, however, allowed the mid-IR spectra to be located approximately on an absolute wavenumber scale (to better than 1.0 cm^{-1}) for comparison with HITRAN data [29, 30]. Spectral components were then identified by comparison with HITRAN and the absolute values given by HITRAN are quoted here.

The output of the DSML was mixed with 60 mJ of residual radiation at 532 nm from the single-mode Nd:YAG pump laser in a KTP crystal phase matched to produce difference frequency generation. The beam diameters of the DSML beam and the 532-nm pump beam were 2.5 and 3 mm, respectively. To minimize the risk of damage to the nonlinear crystal neither beam was focused. It is possible that higher conversion efficiencies could be achieved given the total input energy of 100 mJ by using a higher quality mixing crystal with a higher damage threshold. The output at 3.3 µm, however, provided a pulse of up to 1 mJ with a duration estimated to be ∼4 ns giving an intensity more than sufficient to generate signals with good signal-to-noise ratio. The IR detector had insufficient bandwidth to allow a more precise determination of the pulse duration. The beam profile at the interaction region was approximately Gaussian with a diameter of about 3.5–4.0 mm.

The spectral bandwidth of the mid-IR output had also to be estimated as no instrument of sufficient resolution in the mid infrared was available. The 'effective' bandwidth of the mid-infrared radiation was estimated by recording the spectral profile of an isolated absorption line in methane at low pressure by scanning the DSML across the line. A similar procedure was used by Lucht and co-workers to estimate the line width of the idler beam from their OPG/OPO system [20]. In their case a low-pressure absorption spectrum of an acetylene line at 6518.4858 cm^{-1} was recorded and the laser line width estimated from the convolution of the laser and absorption line shapes. In the present work the Q(14) line in methane was recorded at low pressure (∼10 mTorr) where the absorption line shape is dominated by Doppler broadening leading to a Doppler width of 0.0092 cm^{-1}. The spectral profile of the mid-IR output is unknown and so was assumed to be Gaussian. Thus, the effective absorption line shape will be a convolution of two Gaussians—the laser profile and the Doppler-broadened absorption line. An estimate of the mid-IR laser line width can then be found by deconvolution. The linearity of the frequency axis was checked by comparing wavelength values measured by a four-stage Fizeau interferometer (Cluster LM007) with values of the methane absorption lines in the HITRAN data base. The absorption spectrum (absorption coefficient proportional to optical depth) of a single isolated line is shown in Fig. 2. The best-fit line shape yielded an effective width of the laser

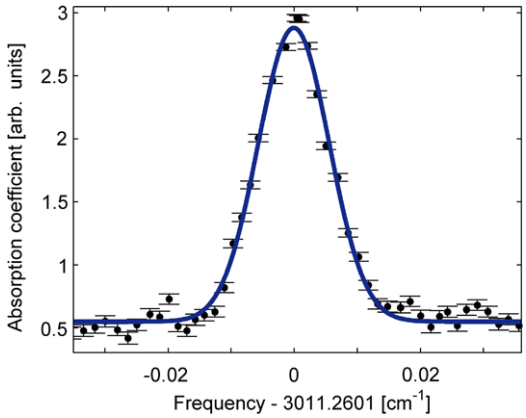

Fig. 2 Absorption line profile of the Q(14) line in methane obtained by scanning the DSML. The spectrum was recorded at low pressure (∼10 mTorr) where the absorption line shape is dominated by Doppler broadening. The *solid curve* is a Gaussian profile fitted to the data. The line width of the laser, 0.011 cm^{-1}, is derived by deconvolving an assumed Gaussian profile for the Doppler-broadened absorption line of 0.0092 cm^{-1}

spectrum of 0.011 cm^{-1}. This is consistent with the combined effects of the DFG process involving two single-mode fields, DSML and seeded Nd:YAG laser, with finite bandwidths (∼0.006 cm^{-1}) and pulse shortening of the infrared pulse relative to the two visible laser pulses arising from the nonlinear difference frequency mixing process. (The line width of the seeded Nd:YAG laser, according to the manufacturer's specification, is in the range 0.003–0.006 cm^{-1}. Single-mode operation was verified by observing the pulse shape and spectrum of the laser at the second-harmonic wavelength.)

The intensity of the pump (and probe) beams was adjusted using a half-wave plate and linear polarizing prism. IR-PS signals were obtained over a range of intensities to determine the saturation levels in the experiment. Operating in the unsaturated regime IR-PS and IR-DFWM signals were generated in pure methane or methane/nitrogen mixtures. Relative frequency detunings were measured using the multiple Fizeau interferometer. The spectra obtained by scanning over multiple transitions were put on an absolute wavenumber scale by comparison with published values from the HITRAN database.

For the IR-PS experiments the degree of polarization and its control are crucial to achieving a good signal-to-noise ratio. Polarizers constructed of YVO_4 were used to control the polarization of the pump and probe beams. The crossed polarizers in the probe beam were measured to have an extinction of 2.6×10^{-7}.

Alignment of the beams for IR-PS and IR-DFWM was facilitated by using a HeNe laser, operating at 0.632 µm, to track the infrared pump, probe and signal beams. The HeNe laser was made collinear with the infrared beam by alignment of both beams through a set of two pinholes.

The signals in both IR-PS and IR-DFWM experiments were detected using an InSb detector cooled by liquid nitrogen (Cincinnati Electronics).

3 Infrared polarization spectroscopy

IR-PS signals were recorded in the Q-branch and the R-branch of the ν_3 band of CH_4. Assignments here follow the notation of [31, 32] indicating the branch, rotational quantum number, J, symmetry species, C, and energy ordering index, N. The dependence of the IR-PS signal on pump beam intensity was measured using the $Q(3)F_2,1$ line at 3018.3585 cm^{-1} where the nearest neighbouring lines lie at between 0.1 and 0.2 cm^{-1} compared to the laser line width of ~0.01 cm^{-1}. The signal intensity was measured as a function of the pump intensity by varying the pump beam intensity using crossed polarizers. The data is shown in Fig. 3. The straight line of slope 2 shows the expected quadratic dependence of the signal at lower pump power. The deviation at higher powers shows the onset of saturation. Other work has studied saturation of the R(3) line which has three components $R(3)A_2,1$, $R(3)F_2,1$ and $R(3)F_1,1$ separated by 0.04 cm^{-1}, which is comparable to the line width of the laser used, 0.04 cm^{-1} [8]. The signals generated at lower pump intensity were reported to follow a power law of 1.5 rather than the expected value of 2 as in the present work. The quadratic dependence in the present work may be a result of the narrower laser line width relative to the line separations—a factor of 10 in the present work compared to a factor of about 1 in [8]. The use of a relatively more isolated transition also avoids possible coherent interference effects of neighbouring transitions. Other factors such as difference in beam shape could also account for the difference in power dependence observed. Saturation is evident in Fig. 3 for intensities above 100 μJ corresponding to a saturation intensity I_{sat} of approximately 3 MW/cm^2, which is similar to that observed in [8].

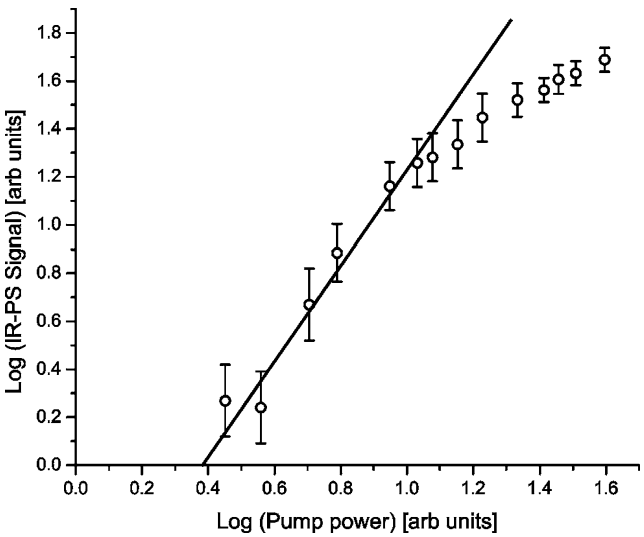

Fig. 3 Log/log plot of IR-PS signal intensity vs pump power. The *solid line* is a straight line of slope of 2 indicating a quadratic dependence of signal on pump power. A pump energy of approximately 100 μJ in a 4-ns pulse corresponds to a log(pump power) = 1. The deviation from the quadratic dependence, i.e. onset of saturation, begins at pump energies >100 μJ (beam sizes are given in the text)

In the data presented here intensities at or below the value of I_{sat} were used consistent with maintaining an adequate signal-to-noise ratio. Signals were initially generated with $I \sim I_{sat}$ in 5 Torr of pure methane. The maximum signal-to-noise ratio achieved was 1400:1, although 150:1 was more typical. IR-PS spectra were recorded over selected sections in the region of 3010 to 3050 cm^{-1}. A typical section around 3018 cm^{-1} is shown in Fig. 4 recorded with 6 Torr methane. The signal-to-noise ratio in this case is 150:1. The solid line consists of Gaussian profiles fitted to the data since the lines are predominantly Doppler broadened at low pressure. The single $Q(3)F_2,1$ line at 3018.3585 cm^{-1} is shown in more detail in Fig. 5a. Figure 5b shows a high-resolution scan of several closely spaced lines, Q(6)E,1, $Q(6)F_2,1$ and $Q(7)A_2,1$, at 3016.4581, 3016.4888 and 3016.4977 cm^{-1}, respectively. The lines are separated by 0.0307 and 0.0089 cm^{-1}; the latter separation is comparable to the Doppler width and at the limit of the resolution of the laser system. The data points are averaged values over 50 laser pulses and the error bars indicate the standard error in the data.

Assuming a Doppler width of 0.0092 cm^{-1}, calculated for the room temperature at which the data was recorded, the residual line width obtained from the best-fit Gaussian curve was 0.015 cm^{-1}. The fact that this width exceeds the estimated laser width is attributed to the effects of absorption and some degree of power broadening. To the authors' knowledge these results represent the highest resolution yet

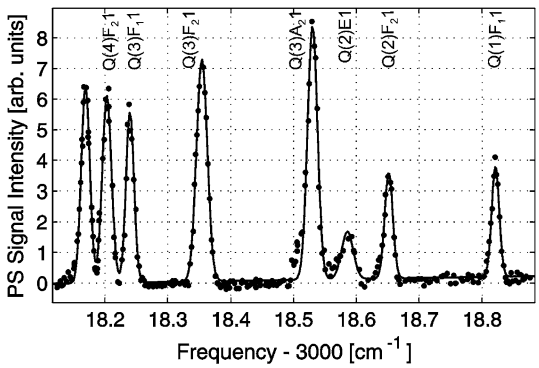

Fig. 4 Part of the IR-PS spectrum recorded in 6 Torr pure methane covering a 0.9 cm^{-1} section around 3018 cm^{-1}. The signal-to-noise ratio in this spectrum is typical at ~150 : 1. The *solid line* consists of Gaussian profiles fitted to the data. Line assignments follow [32]

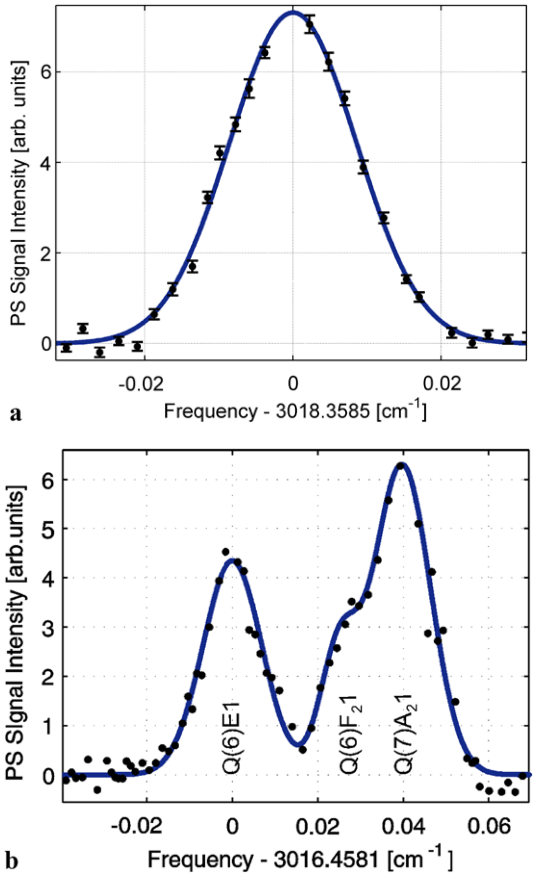

Fig. 5 **a** Expanded view of single IR-PS peak arising from Q(3)F_2,1 transition at 3018.3585 cm^{-1}. Data points are averages of 50 consecutive pulses and the *error bars* indicate the standard error. **b** Expanded view of the closely spaced three-component multiplet, Q(6)E,1, Q(6)F_2,1 and Q(7)A_2,1, with spacings of 0.0307 and 0.0089 cm^{-1}. The spacing of the two closest components is approximately equal to the Doppler width of 0.0092 cm^{-1}. *Solid lines* are fitted Gaussian profiles. Line assignments follow [32]

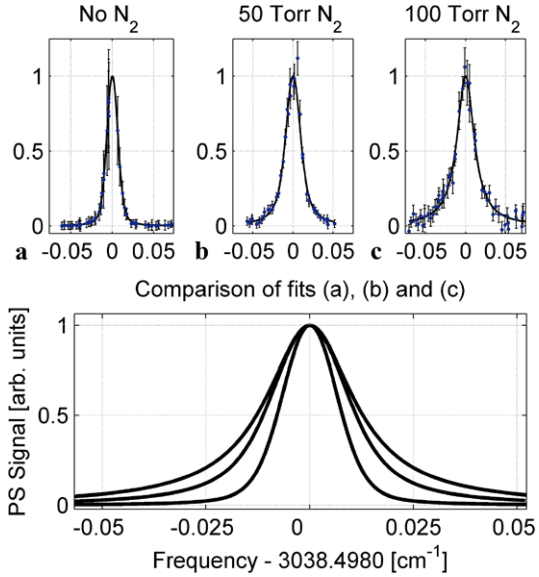

Fig. 6 Pressure broadening of IR-PS signal on the R(1)F_1,1 line at 3038.4980 cm^{-1} for 5 Torr methane in nitrogen mixtures. **a**–**c** Voigt line shapes recorded with nitrogen pressures of 0, 50 and 100 Torr, respectively. The *lower figure* shows the fitted Voigt line shapes for comparison

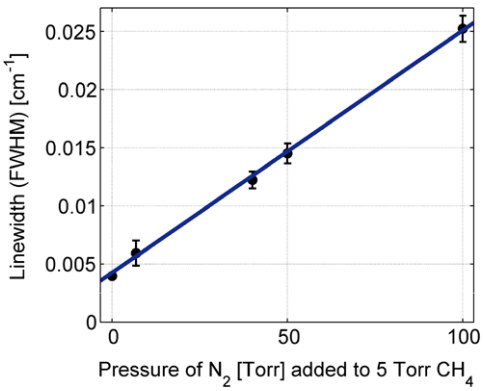

Fig. 7 Plot of IR-PS line width vs. pressure of added nitrogen for the data of Fig. 6 showing linear dependence on nitrogen pressure. The broadening coefficient of 0.00021 $cm^{-1}\,Torr^{-1}$ is derived from the best-fit straight line to the data shown

obtained for polarization spectroscopy in the mid infrared using a pulsed laser.

The effects of collision or pressure broadening are illustrated in Fig. 6, which shows the IR-PS line shape for the relatively isolated R(1)F_1,1 line at 3038.4980 cm^{-1}. The signals were obtained from pure methane at 5 Torr and with the addition of up to 100 Torr nitrogen. The Lorentzian contribution to the Voigt profiles was measured over the range 0–100 Torr of nitrogen and the collisional width as a function of pressure is shown in Fig. 7. The slope of the best-fit straight line yields a pressure broadening coefficient of 0.00021 ± 0.00005 cm^{-1}/Torr, in agreement with published values [28–30]. This data shows a residual width of 0.0043 cm^{-1}, which may be due to effects of residual self broadening, power broadening and absorption.

It was found that to maintain an acceptable signal-to-noise ratio of >100:1 it was necessary to use high concentrations N of methane, and hence relatively high partial pressures of the order of 1–5 Torr in the mixtures with N_2. When lower pressures were used the signal-to-noise ratio deteriorated rapidly as a consequence of the N^2 dependence of the signal.

The signal-to-noise in PS experiments is critically affected by the extinction of the crossed polarizers. Careful alignment of the two polarizers was necessary to ensure perfect crossing and so achieve the maximum extinction of 2.6×10^{-7} quoted above. Uncrossing of the polarizers arises from drifts in alignment of beam-steering optics and opto-mechanical mounts holding the polarizers and leads to leakage of the probe light, to increase in background noise and

to dispersion-shaped line shapes which complicate spectral fitting [27]. In practice, the optical mounts suffered from movement due to thermal changes and physical vibrations external to the experiment. As a result the IR-PS spectra could change in character during the extended times necessary to acquire data over a wide spectral scan. Such changes limit the ability to derive quantitative information from relative intensities of spectral lines.

4 Infrared degenerate four wave mixing spectroscopy

IR-DFWM is often considered to be experimentally more difficult than IR-PS owing to the need to align three input beams rather than the two involved in IR-PS. Alignment of two pump beams and a probe beam in a forward-folded boxcar geometry [33] has been shown to be facilitated by the use of fixed plate beam splitters [34, 35]. Reliable and robust alignment has been achieved in this way to allow DFWM signals from combustion-generated NO to be recorded in a firing SI (spark ignition) engine [36]. The use of parallel-sided optical flats to generate multiple beams from surface reflections is complicated in the mid infrared by the high absorption of infrared radiation in the usual optical materials used in the visible region, e.g. glass and quartz. An attempt to overcome this absorption was made by using thin quartz beam splitters and mirrors held on the surface of a parallel-sided steel substrate with holes drilled to transmit the laser beams. Using this scheme weak IR-DFWM signals were generated in the forward-folded boxcar geometry. The weakness of the signals was attributed to imperfections in the parallelism of the steel substrate and consequent imperfect overlap of the two pump and probe beams in the interaction region. In principle this method should work if the reflecting surfaces are coated on the surface of an optically polished accurately parallel-sided substrate that is transparent in the mid infrared, e.g. calcium fluoride.

In the present work therefore it was found convenient to use the counter-propagating geometry and this was found to be reliable and stable. In practice it is relatively easy to align both pump beams by simply retro-reflecting the pump beam through a system of two apertures. The probe beam is then easily overlapped with the pump beams and in effect the arrangement is no more difficult than overlapping of only two beams. This geometry also offers a reduction in the Doppler broadening in the IR-DFWM line shapes. The mirror used to produce the retro-reflected pump beam is placed approximately 30 cm from the interaction region to ensure that there is sufficient temporal overlap of the forward- and backward-going pulses of duration ∼4 ns. The distance back to the DFG crystal however exceeds the length of the pulse and so no interference with the mixing process is caused by the counter-propagating pump pulse.

A pump beam pulse energy of up to approximately 100 μJ was used for the IR-DFWM experiments such that the signals were in the unsaturated regime or approaching the saturation value at methane pressures of a few Torr. The dependence of the IR-DFWM signals on pump power was measured using the isolated R(1) line at 3038.4980 cm^{-1} and is shown in Fig. 8. The solid line is a straight line of slope 2 showing the expected quadratic dependence of the signal on pump intensity at lower intensities. The deviation from quadratic dependence for higher pump powers shows the onset of saturation at about the same value as for IR-PS under similar conditions, i.e. about 100 μJ in a 4-ns pulse.

Figure 9 shows an IR-DFWM spectrum of pure methane at 3 Torr indicating an excellent signal-to-noise ratio of 650:1. (This is much stronger than the IR-PS signals using the forward geometry under similar conditions of methane concentration and pressure.) Strong signals and excellent signal-to-noise were maintained even when the methane pressure was reduced to less than ∼10 mTorr. In addition, as seen in Fig. 9, impurities in the methane gas were detected, namely ethylene giving the features indicated by arrows at 3017.555 and 3017.6886 cm^{-1}. (The concentration of ethylene is unknown but the total impurity of *all* species contributed to no more than 0.005% of the volume as specified in the manufacturer's specified assay.) The cell was evacuated using a rotary vacuum pump capable of achieving pressures in the range 1–10 mTorr and strong IR-DFWM sig-

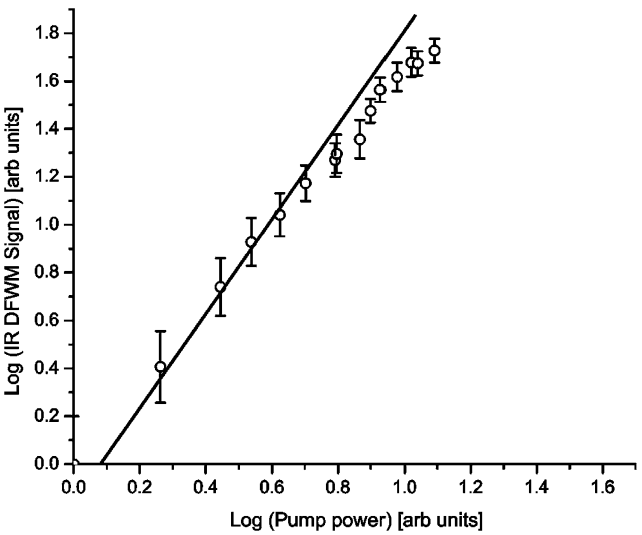

Fig. 8 Log/log plot of IR-DFWM signal vs. pump power on the R(1) line at 3038.4980 cm^{-1}. The *solid line* is a line of slope 2 showing that the signals obey the expected quadratic dependence on pump power up to the onset of saturation. As in Fig. 3 a pump energy of approximately 100 μJ in a 4-ns pulse corresponds to a log(pump power) = 1. The deviation from the quadratic dependence, i.e. onset of saturation, begins at pump intensities >100 μJ similar to that shown in Fig. 3 for IR-PS. Higher pump energies were not used to avoid risk of damage to the DFG crystal

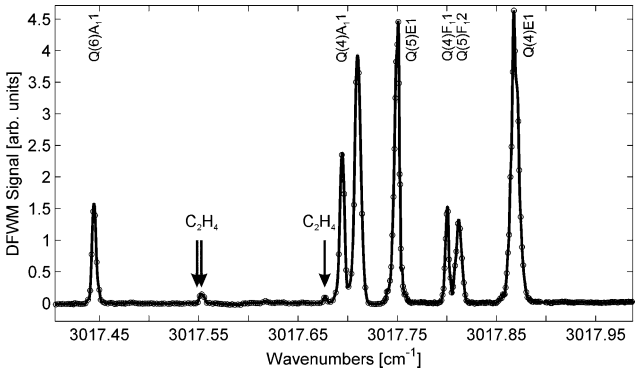

Fig. 9 Part of the IR-DFWM spectrum recorded in 3 Torr pure methane showing a signal-to-noise ratio of ∼650:1 for comparison to IR-PS shown in Fig. 4. Note the detection of impurity lines indicated by the arrows that are identified as from ethylene present at no more than 0.005% of the total. (0.005% is the maximum concentration of all impurity gases present.) The *solid line* is a spline fit to the data. Line assignments follow [32]

nals were still observed. At these concentrations the system would not have provided any detectable IR-PS signals.

Many of the strongest lines in the IR-DFWM spectra exhibit strong absorption at line centre. In the wings of these lines strong signals are generated where the nonlinearity exceeds the absorption but this leads to the appearance of a doublet structure to these lines. The absorption affects the intensity of all three input beams and so has a strong effect on the generated signal. In the presence of such absorption it is not possible to derive quantitative data on relative line intensities. This absorption is a result of using a relatively long path cell in which to conduct these experiments at variable pressures. The use of a flow or jet would reduce these effects [8].

A further, and practically important, effect of the strong line-centre absorption in the present set-up is that the signals no longer follow a simple quadratic dependence on number density. Absorption effects on DFWM were first considered by Caro and Gower [37] in the limit of optically thin conditions. Under these conditions, and for $I < I_{\mathrm{sat}}$, the signal is expected to scale with N^2. DFWM under optically thick conditions has been considered by Ewart and O'Leary [38] who showed that the DFWM reflectivity is modified by a factor of $\exp(-2\alpha_{\mathrm{s}}L)$, where α_{s} is the saturated absorption coefficient, proportional to N, and L is the interaction length in the absorber. As a result the signals can actually increase as N decreases owing to the reduced effect of absorption occurring outside the interaction region. Further decrease of number density leads eventually to a regime where $\exp(-2\alpha_{\mathrm{s}}L) \sim 1$ and a quadratic dependence of signal strength on N is observed. Most of the signals observed in this work are strongly affected by exponential absorption since the path length in the gas cell (100 mm) is much longer than the interaction region (∼10 mm). This explains why signals were observed even at 10 mTorr, which under optically thin conditions would be about five orders of magnitude lower than those observed at 3 Torr.

At the lower pressures the saturation intensity will also be reduced and so some degree of saturation may be evident when using intensities that are unsaturating at the higher pressures. Owing to the dependence of the absorption factor on the degree of saturation, specified by α_{s}, it is not expected that the signal dependence on N will follow a simple quadratic dependence under conditions of strong absorption and partial saturation. These considerations preclude quantitative estimation of the detection limit for IR-DFWM based on the present observations. Future work would eliminate the absorption effects by generating signals in a flow or jet under optically thin conditions using diluted mixtures of CH_4 and buffer gas as in [8].

The IR-DFWM signals were found to be stronger and more reproducible than the equivalent IR-PS signals under similar conditions. IR-DFWM also does not rely on having high-quality polarizing prisms, which are expensive and difficult to manufacture with the required extinction. Consequently, the IR-DFWM signals were not subject to the misalignment effects in polarizing prisms that were a practical difficulty in IR-PS. Furthermore, IR-DFWM can be used to detect species within containers requiring access through window materials that are subject to stress-induced birefringence that would interfere with IR-PS signals. Finally IR-DFWM signals may be analysed using relatively simple analytical models [39–41]. In contrast , complex numerical simulations are usually necessary for quantitative interpretation of IR-PS signals [42].

5 Conclusion

The application of a diode-seeded modeless laser system to polarization spectroscopy and degenerate four wave mixing has been demonstrated indicating that the frequency and pointing stability of the laser are sufficient to make it suitable for nonlinear spectroscopy in the important mid-infrared spectral region. The results show that the system is capable of providing high-resolution spectra using both IR-PS and IR-DFWM. Pressure broadening coefficients derived from line shapes as a function of nitrogen buffer gas pressure were found to agree with literature values.

With this high-resolution system it was found that IR-DFWM provided stronger signals with higher signal-to-noise ratios and greater sensitivity than IR-PS at low concentrations of methane. IR-DFWM was also found to be experimentally easier to implement than IR-PS owing to the latter's sensitivity to misalignment of the infrared polarizers.

References

1. A.C. Eckbreth, *Laser Diagnostics for Combustion, Temperature and Species*, 2nd edn. (Gordon & Breach, New York, 1996)
2. T. Dreier, P. Ewart, Coherent techniques for measurements with intermediate concentrations, in *Applied Combustion Diagnostics*, ed. by K. Kohse-Höinghaus, J. Jeffries (Taylor & Francis, London, 2002), pp. 69–97
3. G. Germann, A. McIlroy, T. Dreier, R. Farrow, D. Rakestraw, B. Bunsenges, Phys. Chem. **97**, 1630 (1993)
4. S. Roy, R. Lucht, A. McIlroy, Appl. Phys. B **75**, 875 (2002)
5. Z. Alwahabi, J. Jetterberg, M. Alden, Opt. Commun. **233**, 373 (2004)
6. T. Settersten, R. Farrow, J. Gray, Chem. Phys. Lett. **369**, 584 (2003)
7. Z. Li, M. Rupinski, J. Jetterberg, Z. Alwahabi, M. Alden, Chem. Phys. Lett. **407**, 243 (2005)
8. Z. Li, M. Rupinski, J. Jetterberg, Z. Alwahabi, M. Alden, Appl. Phys. B **79**, 135 (2004)
9. Z. Li, M. Rupinski, J. Jetterberg, M. Alden, Proc. Combust. Inst. **30**, 1629 (2005)
10. G.J. Germann, R.L. Farrow, D.J. Rakestraw, J. Opt. Soc. Am. B **12**, 25 (1995)
11. D.C. Hovde, J.H. Timmermans, G. Scoles, K.K. Lehmann, Opt. Commun. **86**, 294 (1991)
12. T.D. Raymond, W.J. Alford, A.V. Smith, M.S. Bowers, Opt. Lett. **19**, 1520 (1994)
13. M.J.T. Milton, T.D. Gardiner, G. Chourdakis, P.T. Woods, Opt. Lett. **19**, 281 (1994)
14. G.W. Baxter, M.J. Johnson, J.G. Haub, B.J. Orr, Chem. Phys. Lett. **251**, 211 (1996)
15. G.W. Baxter, H.D. Barth, B.J. Orr, Appl. Phys. B **66**, 653 (1998)
16. G.W. Baxter, Y. He, B.J. Orr, Appl. Phys. B **67**, 753 (1998)
17. G.W. Baxter, M.A. Payne, B.D.W. Austin, C.A. Halloway, J.G. Haub, Y. He, A.P. Milce, J.F. Nibler, B.J. Orr, Appl. Phys. B **71**, 651 (2000)
18. S. Wu, V.A. Kapinus, G.A. Blake, Opt. Commun. **159**, 74 (1999)
19. W.D. Kulatilaka, R.P. Lucht, S.F. Hanna, V.R. Katta, Combust. Flame **137**, 523 (2004)
20. W.D. Kulatilaka, T.N. Anderson, T.L. Bougher, R.P. Lucht, Appl. Phys. B **80**, 669 (2005)
21. Z. Li, M. Afzelius, J. Zetterberg, M. Alden, Rev. Sci. Instrum. **75**, 3208 (2004)
22. M.J. New, P. Ewart, Opt. Commun. **123**, 139 (1995)
23. A. Schocker, A. Brockhinke, K. Bultitude, P. Ewart, Appl. Phys. B **77**, 101 (2003)
24. K. Bultitude, R. Stevens, P. Ewart, Appl. Phys. B **79**, 767 (2004)
25. K. Richard, P. Manson, P. Ewart, Meas. Sci. Technol. **19**, 015603 (2007)
26. C. Wieman, T. Hansch, Phys. Rev. Lett. **36**(20), 1170 (1976)
27. W. Demtroder, *Laser Spectroscopy* (Springer, Berlin, 1981)
28. P. Ewart, Opt. Commun. **55**, 124 (1985)
29. L.S. Rothman, D. Jacquemart, A. Barbe, D.C. Benne, M. Birk, L.R. Brown, M.R. Carleer, C. Chackerian, L.H. Coudert, V. Dana, V.M. Devi, J.M. Flaud, R.R. Gamache, A. Goldman, J.M. Harmann, K.W. Jucks, A.G. Maki, J.Y. Mandin, S.T. Massie, J. Orphal, A. Perrin, C.P. Rinsland, M.A.H. Smith, J. Tennyson, R.N. Tolchenov, R.A. Toth, J. Vander Auwera, P. Varanasi, G. Wagner, J. Quant. Spectrosc. Radiat. Transf. **96**(2), 139 (2005)
30. HITRAN database, http://www.hitran.com
31. A.S. Pine, J. Opt. Soc. Am. **66**, 97 (1976)
32. L. Féjard, J.P. Champion, J.M. Jouvard, L.R. Brown, A.S. Pine, J. Mol. Spectrosc. **201**, 83 (2000)
33. A.C. Eckbreth, Appl. Phys. Lett. **32**, 421 (1978)
34. R.B. Williams, Ph.D. thesis, Oxford University, 1995
35. H. Latzel, A. Dreizler, T. Dreier, J. Heinze, M. Dillmann, W. Stricker, G.M. Lloyd, P. Ewart, Appl. Phys. B **67**, 667 (1998)
36. R. Stevens, P. Ewart, H. Ma, C.R. Stone, Combust. Flame **148**, 223 (2007)
37. R.G. Caro, M.C. Gower, IEEE J. Quantum Electron. **QE-18**, 1376 (1982)
38. P. Ewart, S.V. O'Leary, J. Phys. B, At. Mol. Phys. **17**, 4595 (1984)
39. R. Abrams, R. Lind, Opt. Lett. **2**, 94 (1978)
40. R. Abrams, R. Lind, Opt. Lett. **3**, 205 (1978)
41. R.T. Bratfalean, G.M. Lloyd, P. Ewart, J. Opt. Soc. Am. B **16**, 952 (1999)
42. T.A. Reichardt, R.P. Lucht, J. Chem. Phys. **109**, 5830 (1998)